A few simple rules governing hydrogenation of graphene dots

Cite as: J. Chem. Phys. **135**, 164701 (2011); https://doi.org/10.1063/1.3650693
Submitted: 31 July 2011 • Accepted: 22 September 2011 • Published Online: 24 October 2011

M. Bonfanti, S. Casolo, G. F. Tantardini, et al.

A few simple rules governing hydrogenation of graphene dots

M. Bonfanti,[1] S. Casolo,[1] G. F. Tantardini,[1,2,3] A. Ponti,[2] and R. Martinazzo[1,2,3,a)]
[1]*Dipartimento di Chimica Fisica ed Elettrochimica, Università degli Studi di Milano, v. Golgi 19, 20133 Milan, Italy*
[2]*Istituto di Scienze e Tecnologie Molecolari, Consiglio Nazionale delle Ricerche, v. Golgi 19, 20133 Milano, Italy*
[3]*CIMaINa, Interdisciplinary Center of Nanostructured Materials and Interfaces, v. Celoria 16, 20133 Milan, Italy*

(Received 31 July 2011; accepted 22 September 2011; published online 24 October 2011)

We investigated binding of hydrogen atoms to small polycyclic aromatic hydrocarbons (PAHs)—i.e., graphene dots with hydrogen-terminated edges—using density functional theory and correlated wavefunction techniques. We considered a number of PAHs with three to seven hexagonal rings and computed binding energies for most of the symmetry unique sites, along with the minimum energy paths for significant cases. The chosen PAHs are small enough to not present radical character at their edges, yet show a clear preference for adsorption at the edge sites which can be attributed to electronic effects. We show how the results, as obtained at different levels of theory, can be rationalized in detail with the help of a few simple concepts derivable from a tight-binding model of the π electrons.
 [doi:10.1063/1.3650693]

I. INTRODUCTION

Graphene, the recently discovered two-dimensional form of carbon,[1] is a promising material for a future carbon-based nanoelectronics. Its peculiar $\pi - \pi^*$ electronic band structure, with a linear energy dispersion close to the Fermi level, introduces subtle quantum pseudo-relativistic effects in the low-energy charge carrier dynamics which hugely impact on the transport properties.[2–4] This results, e.g., in a robust anomalous quantum Hall effect,[5,6] a universal conductivity minimum[7] and ballistic transport which can reach the micrometer scale.[8] From a practical point of view, the substrate thickness, the high mobility of its charge carriers and their (high-field) high saturation velocity represent attractive features for the chip-makers. Nanostructuring, however, is needed for applications, e.g., for devising graphene-based logic transistors where a band-gap is needed to achieve high operational on-off ratios. Graphene nanoribbons (GNRs) can be cut which show either semiconducting or metallic properties, the latter coming with edge states of unusual magnetic properties, possibly leading to carbon based nanomagnets.[9,10] Likewise, Graphene dots (GDs) can be designed to have specific electronic structures and transport properties, by acting just on their shape and their connectivity. GDs have been suggested for realizing spin qubits,[11] spin filters[12,13] and spin-logic devices,[14] and proposed as biomedical imaging agents[15] and light absorbers for photovoltaics.[16] Transport properties have been measured on a variety of dot devices carved entirely from graphene by high-resolution electron-beam lithography.[17]

Most of these properties arise entirely from the π electrons and remain unaltered when saturation of the dangling σ bonds occurs, e.g., in forming polycyclic aromatic hydrocarbons (PAH). The latter offer an enhanced chemical stability, and their nanostructuring (energy level arrangement, interfacing with other materials, etc.) can be realized with the help of well-developed carbon chemistry methods. They have been used as building blocks for atomically precise nanoribbon fabrication[18] and, in principle, may form the basis for a bottom-up approach to realize arbitrarily complex carbon-nanostructures. PAHs have also been investigated in many other fields, from petroleum chemistry to astrochemistry. For instance, in the interstellar medium, i.e., the extremely rarefied medium which fills the space between stars, the observed abundance of molecular hydrogen cannot be explained by direct gas-phase routes involving *H* atoms only, rather is believed to occur on the carbonaceous surface of dust grains[19,20] and small carbonaceous particles. PAHs, which are estimated to lock up ≈15% of the interstellar carbon, have been suggested as possible catalysts for H_2 formation.[21–23]

In this work, we investigate the reaction of atomic hydrogen with a number of PAHs, complementing previous related studies[21,23–26] which showed preference for addition at the edges of selected PAH molecules. One of the main aim of this study was to emphasize the importance of substrate relaxation ("geometric") effects in determining a preference towards the edges. To this end, we selected substrate PAH molecules with relatively small (sub-nanometer) dimensions, in such a way to prevent any enhanced chemical reactivity at the edges due to a true radical character (single occupation of a semilocalized edge state), as it occurs for instance at the edges of wide zigzag GNRs. However, as we shall see in the following, some edge localization is *always* present. This provides an enhancement of the edge reactivity which is of purely electronic origin and can be easily understood in terms of a few concepts derivable from a tight-binding (Hückel) model for the π electrons.

a)Electronic mail: rocco.martinazzo@unimi.it.

In addition, depending on the number of carbon atoms available for the π electron system and their connectivity, the systems considered can also show a marked *sub*lattice preference due to the "alternating paths" followed by (unpaired) itinerant electrons in graphenes (i.e., due to the presence of staggered midgap states). This is similar to graphene,[27,28] where these states form the basis for a preferential sticking mechanism[29,30] forming *para*-dimers (i.e., two H atoms on opposite corners of the same ring). We, therefore, distinguish two classes of PAHs according to whether the number of sites in each sublattice is balanced or not, and show how a final set of rules governing the site reactivity results from the interplay of different electronic effects. The basic concepts underlying these rules equally apply to larger systems, and thus allow one to easily predict the chemical reactivity of sp^2 carbon nanostructures with monovalent species forming covalent bonds with the substrate.

Importantly, in the present study we also take advantage of the modest size of the systems investigated, and exploit the unique opportunity of assessing the quality of the results of commonly used density functional theory (DFT) methods in investigating chemically derived graphene structures. This is done here by complementing the DFT data with those obtained by using more accurate correlated wavefunction techniques. *En passant*, we briefly discuss the magnetic properties of pristine and hydrogenated PAHs, which turn out to be well predicted by Lieb's theorem,[31] in agreement with previous studies on triangularly and hexagonally shaped GDs (Ref. 32) and other defective graphenic structures.[27,28]

The paper is organized as follows. Section II introduces some basic properties of π-conjugated carbon systems which underlie the presentation of the results given in Sec. IV, thereafter Sec. III has provided the computational details of our calculations. Section V summarizes and concludes.

Notice that in the following we adopt a surface science terminology, whereby "adsorption to the substrate" (here meant to be chemisorption) is used interchangeably with "binding to the molecule".

II. BASIC PROPERTIES OF π ELECTRONS IN sp^2 CARBON STRUCTURES

Carbon sp^2 structures such as graphene, GNRs, and GDs are characterized by a *bipartite* lattice where two distinct sublattices, A and B, can be identified such that each A site is connected to B sites only and vice versa. This property has long been noticed in the chemical literature[33,34] where these systems are known as *alternant hydrocarbons* and sites are labeled as "starred" ($\star$) and "unstarred"($\circ$). It has important consequences in the one-electron spectrum if, as it is the case for such structures, the transfer (hopping) energies beyond the nearest neighbors are of secondary importance and the orbital overlap can be neglected. Under such circumstances, indeed, it is not difficult to prove that the tight-binding (TB) Hamiltonian for the p_z orbitals of the π electron system has a simple symmetry, as first shown by Coulson and Rushbrooke.[33] Such Hamiltonian reads as

$$H^{\mathrm{TB}} = \sum_{\langle i,j \rangle} t_{ij} a_i^\dagger b_j + h.c. = H_{AB} + H_{BA},$$

where $a_i(a_i^\dagger)$ annihilates (creates) an electron in site i of the sublattice A (similarly for $b_j(b_j^\dagger)$ and B sublattice sites), t_{ij} is the hopping between sites i and j, and the on-site energy (the energy of an isolated p_z orbital) has been set to zero. Bipartitism is responsible for its (off-)block structure—as emphasized here with the introduction of H_{BA} and H_{AB} which collectively describe the transitions $A \rightarrow B$ and $B \rightarrow A$, respectively—and easily leads to a symmetric spectrum around $\epsilon = 0$. The latter is also the position of the Fermi level with one electron per site (half-filling), and for this reason the above symmetry is also called electron-hole symmetry. In conjunction with the spatial symmetry, the presence of such symmetry is at the origin of the conically shaped band structure of graphene close to the Fermi level,[28] with interesting consequences on band-engineering[35,36] and on the chemical reactivity.[27] Here, to clarify the connection with chemical reactivity—along the lines of frontier molecular orbital theory[37]—we focus on some simple results on the *shape* of low-energy (i.e., close to the Fermi level) orbitals that directly follow from such electron-hole symmetry. These results bridge traditional studies on benzenoids to graphene theory.

A. Edge localization and hypercoordination

Low-energy orbitals show a marked tendency to localize on edge sites, as can be easily seen at the tight-binding level. To this end, we perform a lattice "renormalization"[35,38] and focus on one sublattice only (say A) and on the "renormalized" Hamiltonian $\tilde{H} = H_{AB} H_{BA}$. The renormalized energies $\tilde{\epsilon}_i$ are simply related to the eigenvalues[39] $\epsilon_i^{\pm}$ of H^{TB}, namely $\epsilon_i^{\pm} = \pm\sqrt{\tilde{\epsilon}_i}$, hence the ground state of the renormalized system corresponds to the highest occupied/lowest unoccupied molecular orbital (HOMO/LUMO) pair of the original system. The renormalized lattice is a triangular lattice (the sublattice A of the original system) with hopping t^2 [assuming $t_{ij} = t$ for simplicity] and on-site energies $t^2 Z_i$, where Z_i is the coordination number of the ith A site in the original lattice. An edge *necessarily* has undercoordinated ($Z = 2$) sites, hence the ground state of the renormalized lattice naturally tends to localize on these sites which present the lowest on-site energy; the same holds for the HOMO/LUMO pair of the original π system in which we are interested. In the following, we name E these two-coordinated edge sites, to distinguish them from those three-coordinated sites which are also present at an edge (F sites), see Fig. 1. Importantly, we expect that low-energy orbitals localize on E sites and, among these, on those sites which show the largest number of undercoordinated neighbors in the renormalized lattice (or, equivalently, next-to-nearest E neighbors in the original lattice) to hybridize with. As is shown in the following, this latter number turns out to be an important parameter ruling the reactivity of the edge sites; for this reason we call it the *hypercoodination*

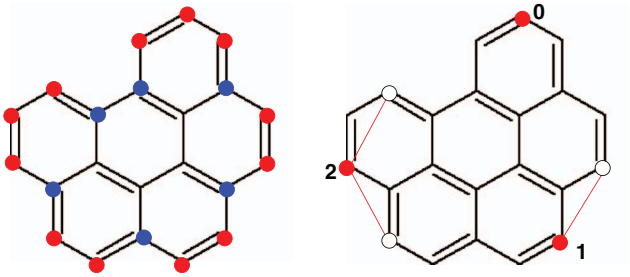

FIG. 1. (Left) Two- (red) and three- (blue) coordinated edge sites in the benzo[ghi]perylene molecule (*E* and *F* sites in the main text). (Right) *E* sites having different hypercoordination numbers (as indicated), along with their hypercoordinated partners (white circles).

number (ξ). Figure 1, right panel, reports some illustrative cases.

B. Midgap states and spin alignment

Obviously, energy levels at $\epsilon = 0$, if present, play a major role at half-filling in determining the reactivity and the magnetic properties of the GDs. It is instructive to see when this situation occurs, as this adds further constraints on the spatial behaviour of the low-energy orbitals. In general, the number of these "midgap" states is determined by the site-connectivity but their occupancy (spin-alignment) is solely determined by the *sublattice imbalance*. This follows from a rigorous result proved by Lieb[31] for the realistic (repulsive) Hubbard model having H^{TB} above as one-electron Hamiltonian: Lieb's theorem states that at half-filling the ground state spin S is given by $S = |n_A - n_B|/2$, where n_A and n_B are the number of sites in the sublattice A and B, respectively.

Typically, the number of midgap states matches the sublattice imbalance—and Lieb's theorem becomes a sort of Hund's rule—since this is enough to allow for $|n_A - n_B|$ linearly independent eigenvectors of H^{TB} at zero-energy, all with *null* amplitudes on the minority sublattice sites (see, e.g., Ref. 40). This is a simple algebraic result. Indeed, let $n_A > n_B$ and $|\psi\rangle = \sum_i \alpha_i |a_i\rangle$ be a trial solution for a zero-energy state (here $|a_i\rangle = a_i^\dagger |0\rangle$ and similarly for $|b_i\rangle$). Then, the condition $\sum_i \langle b_j|H|a_i\rangle \alpha_i = 0$ must hold for $j = 1, \ldots n_B$, which is a set of n_B equations for the $n_A > n_B$ unknowns α_i having (at least) $n_A - n_B$ linearly independent solutions. This also shows that zero-energy ψ's *localize on the A lattice sites*.

More generally, the concept of *non-adjacent* sites in a N-site bipartite system helps counting the number of midgap states.[41–43] We say that two sites are non-adjacent if they are not bound (connected by a transfer integral) to each other; for instance, two sites on the same sublattice are non-adjacent. Clearly, there exists a maximal set of non-adjacent sites and we call α the sites in this set, and β the remaining ones (n_α, $n_\beta = N - n_\alpha$ in number, respectively). Each site α binds at least one site β, otherwise it would represent a completely isolated site. Arranging one electron per site, however, we can form at most n_β bonds at a time, and therefore we are left with $\eta = n_\alpha - n_\beta$ unpaired electrons. Equivalently, we end up with $\eta = 2n_\alpha - N$ midgap states *localized on the maximal set of non-adjacent sites*. Rigorously speaking,[42] for a generic (bipartite) system this is only a lower bound to the number of zero energy states, $\eta \geq 2n_\alpha - N$, since there may exist further states at zero energy for specific values of the hoppings; they are known as *supernumerary*[41] but cannot occur in hexagonal (benzenoid) systems where $\eta \equiv 2n_\alpha - N$ strictly holds.[42] The case of a sublattice imbalance discussed above is a special result of this counting rule which, as is evident from the discussion above, can be equivalently re-phrased[41] by defining η to be the number of unpaired electrons in the Lewis structure(s) with the *maximum* number of π (i.e, double) bonds (*principal resonance structures*).

We thus see that, in addition to the edge localization discussed above, depending on the number of sites and their connectivity, there may exist *topological* constraints which force the carbon sp^2 system to have zero energy states. The latter localize on specific lattice positions which are easily identifiable by inspection.

C. The systems

In the following, we mainly focus on structures where the sublattice imbalance is the only source of midgap states, and call them *balanced* ($S = 0$) or *imbalanced* ($S > 0$), accordingly; in particular, only structures with one unit of imbalance are considered, i.e., they all have $S = 1/2$, as suggested by Lieb's theorem and confirmed by our calculations. The considered structures are shown in Fig. 2, together with a labeling system for the sites investigated, which distinguishes the (two-coordinated) edge sites from the graphitic sites, *E* and *G* in Fig. 2. Sites at the edges which are three-coordinated (*F*) are in between the two categories and will not be considered in the following. With this exception, all the symmetry unique sites were investigated for binding of a H atom, with the methods described in Sec. III.

Notice that Fig. 2 further distinguishes those edge sites which have the largest possible hypercoordination number ($\xi = 2$) with a prime and, where appropriate, identifies with a star the majority sites (either edge or graphitic) where the midgap states are expected to localize. As is shown in the following, these labels help identifying the sites with the highest hydrogen affinity (i.e., the sites with the largest binding energy and the smallest barrier to binding).

III. COMPUTATIONAL METHODS

For each of the selected PAH molecules we computed the binding energy of a hydrogen atom to the sites labeled in Fig. 2 according to

$$E_{bind} = E_{\mathrm{PAH}} + E_{\mathrm{H}} - E_{\mathrm{PAH\text{-}H},}$$

with two different electronic structure methods. PAH structures were optimized at the (unrestricted) DFT level using the popular B3LYP hybrid exchange-correlation functional with Dunning's double-valence, atom-centered basis set of the correlation-consistent type (cc-pVDZ), as implemented in GAUSSIAN 03.[44] On the DFT-optimized structures, single-point wavefunction calculations were performed with the same basis-set. These are of the multi-state,

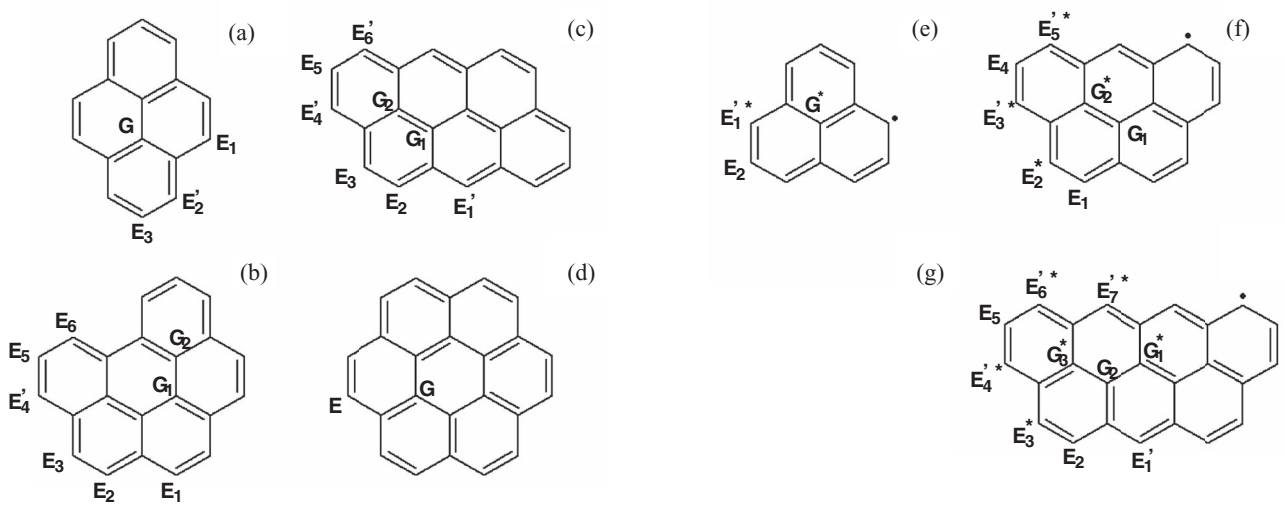

FIG. 2. Balanced ((a)–(d)) and imbalanced ((e)–(g)) PAHs investigated in this work, shown via one of their possible Lewis structures (carbon atoms are at the vertexes of the hexagons, and are meant to be saturated with hydrogen atoms – not shown – if undercoordinated). (a) Pyrene, (b) benzo[ghi]perylene, (c) anthanthrene, (d) coronene, (e) phenalenyl (peri-naphtenyl), (f) benzo[c]pyrenyl, and (g) benzo[c]anthanthrenyl. Also indicated as labeling systems for the adsorption sites considered in this work, E and G for "edge" and "graphitic" sites, respectively. A prime is used for edge sites with hypercoodination number $\xi = 2$ and a star is used in ((e)–(g)) for the majority sites, either E or G, where the unpaired electron (dot) localizes. See Sec. II for details.

multi-reference perturbation theory type according to the scheme of Hirao[45–48] and Nakano[49,50] called multi-configuration quasi-degenerate perturbation theory (MC-QDPT) and implemented in GAMESS.[51] In this scheme, dynamical correlation is introduced in a multi-configurational (MC) wavefunction by properly defining a reference one-electron Hamiltonian based on this wavefunction and computing the second-order perturbation correction. The chosen MC reference wavefunction was of the complete active space self-consistent-field type, where n valence electrons are distributed in m orbitals (CAS(n,m) in the following) and self-consistency is reached in a variational optimization. In principle, for the PAHs above a consistent procedure would require to put all the π electrons of the substrate molecules and that of the added H atom in the same number of orbitals. This is of course impracticable for all but the smallest molecules, and we therefore resorted to an orbital localization procedure which takes advantage of the local character of the bond formation process. We started from Pipek-Mezey ROHF localized orbitals[52] and included in the active space, the σ orbital describing the formation of the C–H bond and the π orbitals localized on the sites which are nearest neighbors of the binding site. This gives rise to typical CAS(9,9) or CAS(8,8) MCSCF wavefunctions and active spaces for the perturbation correction. For the smallest PAHs, we performed some convergence tests on the size of the active space, see Fig. 3 for an example. Finally, we also performed plane-wave based periodic DFT calculations with the help of the VASP code,[53,54] with parameters similar to those used in our previous works[27,55] but adapted to a cluster calculation. Briefly, we adopted a 20 Å×20 Å×20 Å cell and a 700 eV energy cutoff, with a 1×1×1 Γ centered k-point grid. Inner electrons were frozen by the projector augmented wave[56,57] approach, and exchange-correlation effects were handled in the generalized gradient approximation (GGA) with the Perdew-Burke-Eznerhof[58] (PBE) functional in its spin polarized version.

IV. RESULTS AND DISCUSSION

A. Graphitic vs. edge sites

We start by showing the preference for adsorption on the edge sites which was already noted by several authors.[21,23–26] Figure 4 shows the computed binding energy for all the E and G sites of the structures (a)–(d) of Fig. 2, as obtained in the ground state spin manifold of the total system,[59] $S = 1/2$. The DFT results (black histograms) compare very well with the available literature data. For instance, for the pyrene molecule we find 1.53, 1.67, and 1.09 eV for the sites E_1, E_2, and E_3 which compare well with the values 1.50, 1.61, and 1.06 eV recently obtained by Rasmussen *et al.*[26] with a real-space implementation of the DFT-PBE level of theory.

Clearly, a striking difference between E and G sites is apparent from Fig. 4: binding energies at an E site can be as large as twice the binding energy for a G site. The latter,

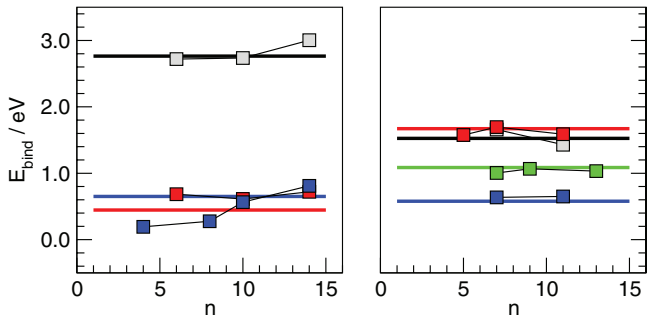

FIG. 3. Convergence tests on the active space used in the MCQDPT calculations. The energies for H atom adsorption are reported for different sites as functions of the number n of active electrons in a (n, n) correlation scheme. (Left) gray, red, and blue symbols for sites E_1, E_2, and G of the phenalenyl radical (structure (e) in Fig. 2). (Right) gray, red, green, and blue symbols for sites E_1, E_2, E_3, and G of pyrene (structure (a) in Fig. 2). Horizontal lines mark the values obtained at the DFT level.

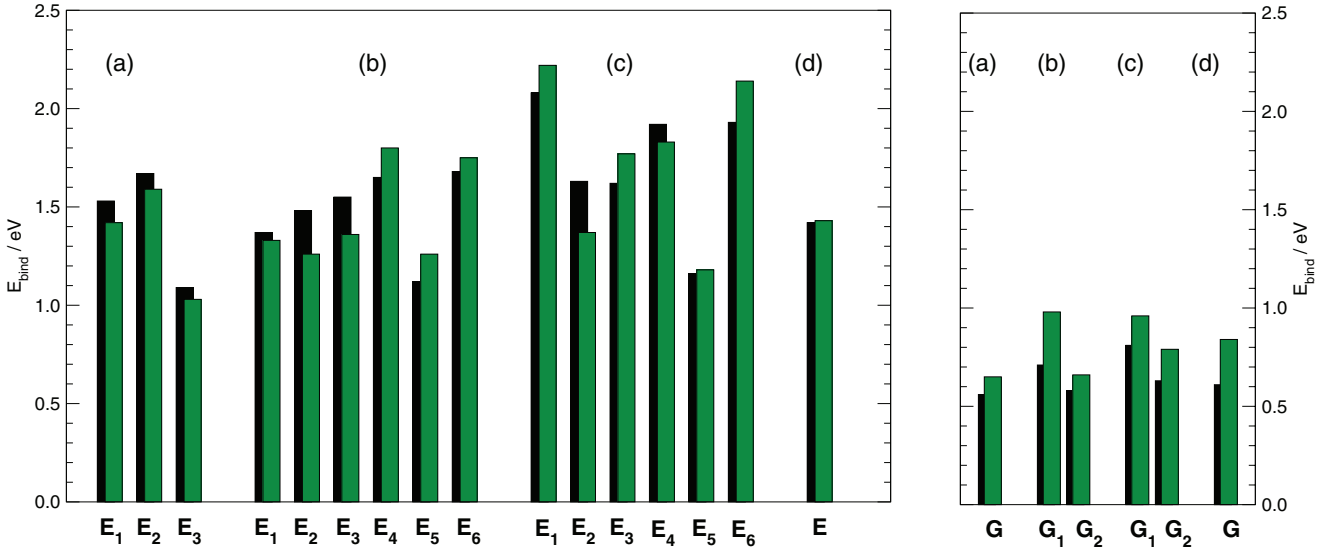

FIG. 4. Binding energies for E (left) and G (right) sites in the structures ((a)–(d)) of Fig. 2. DFT and MCQDPT results are represented as black and green histograms, respectively, according to the labeling system of Fig. 2.

on the other hand, compare rather well with the value of the hydrogen atom adsorption energy in graphene[27,60,61] and graphite.[61,62] This simple finding, together with a corresponding behaviour for barrier energies to be discussed below, already suggests that the edges of realistic samples could be active sites where hydrogenation starts and propagates into the bulk.

B. Geometric vs. electronic effects

Before analysing the results in details, we show here that "geometric" effects *per se* cannot explain the different behaviour of edge and inner sites evident in Fig. 4. Binding of a H atom on a sp^2 carbon atom requires a $sp^2 \rightarrow sp^3$ rehybridization which leads to a tetrahedral reorganization of the bonding partners, as is shown in Fig. 5(a) for the case of the coronene molecule. Without such re-arrangement of the local environment no binding would occur: a local substrate relaxation is essential to "prepare" the electronic structure for binding, but this too is affected by the overall electronic structure which is always dominated by molecular orbitals spreading all over the molecule.

A simple (but wrong) argument would suggest that the *same* local re-arrangement which occurs upon bonding (but *without* the H "probe") requires *less* energy for an edge than for an inner carbon atom, since in the first case at least one of the bonding partners is a monovalent species not embedded in the molecular network. We can define this *reorganization* energy as

$$E_R = E^*_{eq}(\mathrm{PAH}) - E_{eq}(\mathrm{PAH}),$$

where E_{eq}(PAH) is the energy of the pristine molecule in the equilibrium configuration and E^*_{eq}(PAH) is the energy of the molecule in the same distorted configuration that it takes when binding the H atom. In contrast to the expectation above, we find that E_R for an E site is always *larger* than that for a G site. For coronene, for instance, we obtain 1.40 eV and 1.04 eV, respectively, at the DFT level of theory; and similar values are found for all the structures considered in this work: the reorganization energy is $\sim$1.4 $\pm$0.1 eV for E sites and $\sim$1.0 $\pm$0.1 eV for G sites; see, for instance, Fig. 5(b) for the case of the anthanthrene. We thus see that the preference in binding a H atom to an edge site occurs *despite* the larger reorganization energy needed at these kind of sites. This allows us to conclude that this preference is due to the electronic effects introduced in Sec. II.

C. Hypercoordination

Next we discuss the results of Fig. 4 in detail since, apart from the overall behaviour, the binding energies can take quite different values depending on the site they refer to. A closer inspection reveals that the values for the interesting E sites correlate very well with the hypercoordination number introduced in Sec. II: the larger is the hypercoordination, the larger is the binding energy. This can be made evident by reporting the results of Fig. 4 as functions of the site populations p_i of the HOMO; the latter are meant here per spin species, and were obtained by a Mulliken analysis of the molecular orbitals of the pristine molecules, as computed with a restricted Kohn-Sham determinant. This is shown in Fig. 6, where the populations have been normalized to the values they would have if the HOMOs spread over all carbon atoms ($1/N$). Figure 6 shows that the binding energies correlate well with Np_i. The trend is roughly linear and different for the E and the G sites, but we did not attempt to extract any behaviour because of the limited number of data available. More importantly, Fig. 6 shows that the energies correlate well with the hypercoordination number ξ of the site, particularly if the comparison is made between sites of the same molecule. As already emphasized above, this number can be readily obtained by simply inspecting the carbon structure under study.

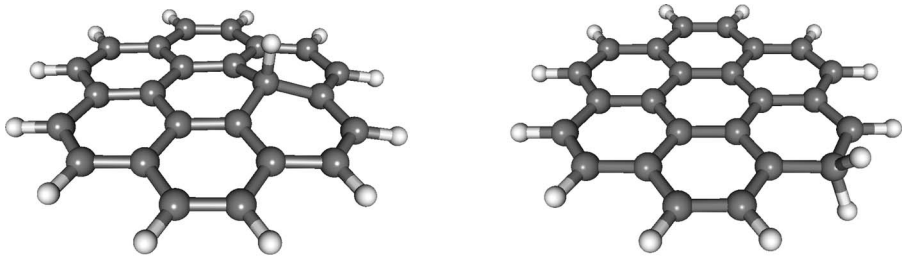

(a)

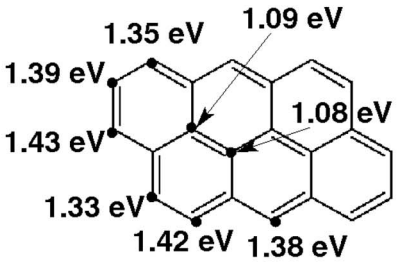

(b)

FIG. 5. (a) Optimized structures for the singly hydrogenated coronene molecule. Left and right panel for adsorption on the *G* and *E* site, respectively. (b) Reorganization energy for adsorption of a H atom in the indicated sites of the anthanthrene molecule.

D. Imbalanced structures

Next we move to the more complicated situation (the doublet structures (e)–(g) of Fig. 2)) where topological constraints lead to the appearance of zero-energy modes and additional "localization." Analogously to the results of Fig. 4, we find also in this case a clear distinction between edge and graphitic sites. This is evident from Fig. 7 where we report the binding energies for the structures (e)–(g) on a larger energy scale than the one used in Fig. 4. This is one of the consequences of the additional electronic effect due to the appearance of the (singly occupied) midgap state: binding of two radical species only requires coupling of their unpaired electrons and is thus typically much more energetic than in the case where a bond has to be broken. A further consequence is a rough splitting of the results into two "branches," according to whether the relevant site belongs or not to the majority set (red and blue blocks of results in Fig. 7). Notice that, according to Lieb's theorem, in the first case the resulting total spin state is a singlet, whereas in the second case is a triplet. This is indeed what we find: Fig. 7 shows that for adsorption of a H atom on a minority site the binding energy in the triplet state is larger than in the singlet. Not shown in the figure, we also checked that adsorption on a majority site occurs more favourably in the singlet manifold; this is true for all cases considered but the site G_1 of structure (g) where we find that H binds more favourably in the triplet state.[63]

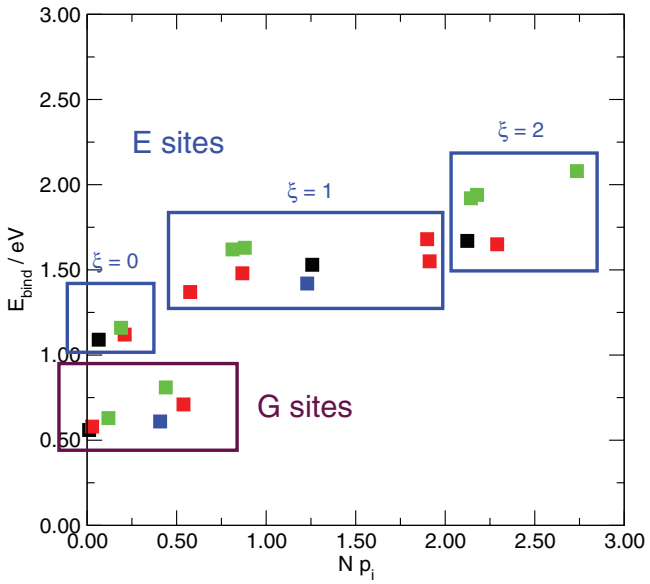

FIG. 6. Binding energies as functions of the site normalized populations of the substrate HOMO. Black, red, green, and blue symbols for structures (a)–(d), respectively. Also indicated the hypercoordination number of the edge sites.

We thus see that, in the case considered in this section, the energy ordering arises from the complicated interplay between coordination, hypercoordination, and topological frustration. For this reason, in plotting the results as functions of the normalized populations, analogously to Fig. 6, we consider separately the majority and the minority sites, reported in the left and right panels of Fig. 8, respectively. We see now that a good correlation between the binding energies and the HOMO populations is found only for the majority sites, nevertheless the hypercoordination number remains a good parameter for establishing the right energy ordering within each category: the binding energy is found to monotonically increase when increasing ξ. In general, majority sites show larger binding energies than minority sites with the same coordination number (i.e., either *E* or *G*) but, even for the same molecule, a large hypercoordination may offset the topological frustration of a

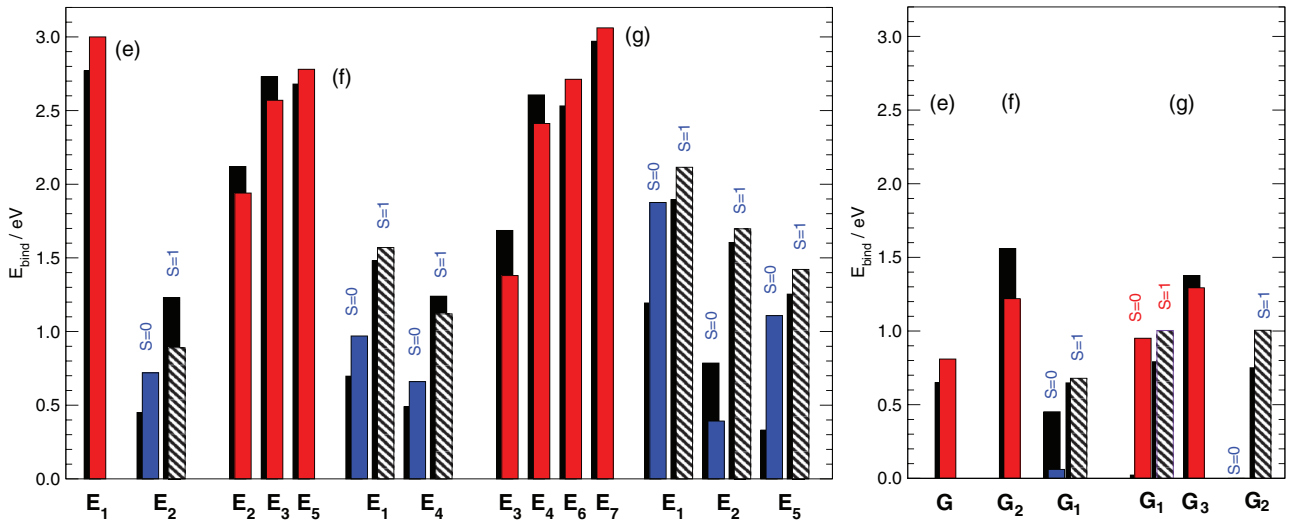

FIG. 7. Binding energies for E (left) and G (right) sites in the structures (e)–(g) of Fig. 2. DFT and MCQDPT results are represented as black and colored histograms, respectively, according to the labeling system of Fig. 2. The color code (for MCQDPT results only) is red for majority and blue for minority sites; occasionally, both the singlet (full color) and the triplet (shaded) spin manifolds have been considered, as indicated. See text for details.

minority site. For instance, the (minority) site E_1 in structure (g) shows a larger binding energy than the (majority) site E_3; notice though that the "expected" ordering is restored if comparison is made between results for the same spin manifold. In general, however, the most favoured (relevant) final hydrogenated structures are always easily identified: they are obtained by binding a H atom to the majority E sites with the largest hypercoordination number.

Notice further that imbalanced structures also arise after a H atom has been adsorbed onto any of the balanced structures (a)–(d), since formation of a CH bond effectively removes one carbon p_z orbital from the π network and thus acts as a vacancy. In this case, hydrogen bonding to form a *dimer* follows the same rules. For instance, Rauls and Hornekaer[23] used DFT-PW91 to systematically investigate hydrogenation of coronene up to saturation. They found that addition of a H atom to the most stable H-coronene structure (i.e., with a first H bound to a E site) is most favoured in the *ortho* edge position, i.e., on the E site which is nearest neighbor to the first adsorption site. This is a majority site with an effective π coordination number $Z = 1$, which would correspond to an additional type of site, "D." Furthermore, five E sites exist in H-coronene with $\xi = 1$ having a large binding energy. Analogous results holds for pyrene, see Rasmussen *et al.*[26]

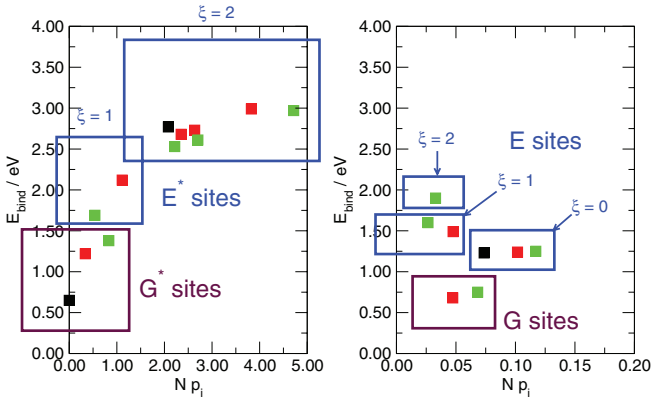

FIG. 8. Binding energies as functions of the site normalized populations of the substrate HOMO. Black, red, and green symbols for structures (e)–(g), respectively. Also indicated the hypercoordination number of the edge sites. Left and right panels for majority and minority sites, respectively.

E. Adsorption profiles

We now look at the full energy profiles (minimum energy paths) for a H atom adsorption, focusing on a few illustrative cases. We show, in particular, that the arguments used so far for the adsorption energies equally apply to the energy *barriers* for the H atom sticking. Thus, the energy ordering rules drawn in Secs. IV A–IV D not only determines the *thermodynamics* but also the *kinetics* of the hydrogenation process.

Hydrogen atom binding is an activated process with an energy barrier which typically prevents adsorption under room temperature conditions.[29,64] For instance, in graphite (graphene) the barrier is ~0.2 eV high and this prevented for some time observation of a chemisorbed hydrogen phase. This barrier is typically linearly related to the binding energy itself,[27] in accordance with the general finding (known as Brønsted–Evans–Polanyi rule) that a larger reaction exothermicity is accompanied by a lower energy barrier. The same applies here, as is shown for the cases of pyrene and coronene reported in Fig. 9, for both an E and a G sites. Such curves have been obtained by fixing the CH distance at the desired value and performing a full structural relaxation of the remaining degrees of freedom at the DFT-B3LYP level of theory. As is evident from the figure, a larger binding energy reflects a smaller adsorption barrier, which can be even almost vanishing when H binding occurs at an edge site. Similar results hold for all the paths considered in this work, i.e., for H atom adsorption on most of the sites considered in Fig. 2. As already noticed above this finding suggests that the edges of realistic samples could be active sites where hydrogenation starts and propagates into the bulk: addition of H atoms

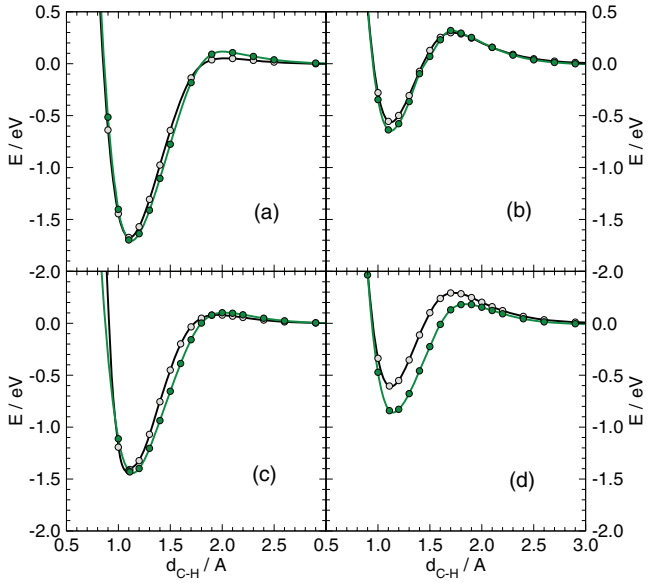

FIG. 9. Hydrogen adsorption paths on pyrene (a)–(b) and coronene (c)–(d), on the left for an edge site and on the right for a graphitic site. Black and green symbols for DFT and MCQDPT results. Lines are spline interpolation to guide the eyes.

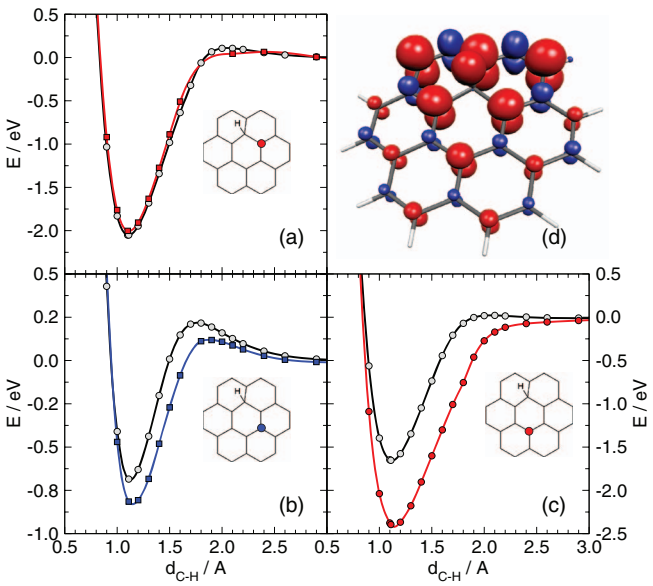

FIG. 10. Adsorption curves for a second H atom in the (graphitic) *ortho* (a), *meta* (b), and *para* (c) positions with respect to a first H atom, as indicated in the insets. Gray and colored symbols for DFT and MCQDPT results, respectively, and lines are spline interpolation to the data for guiding the eyes. Panel (d) shows the spin density of the H-coronene substrate with a H atom adsorbed on a *G* site.

to *E* sites modifies the sublattice imbalance and at the same time effectively converts a number of *F* (*G*) sites into *E* (*F*) sites.

F. Correlation level

Finally, we focus on some technical aspects concerning the treatment of electron correlation. Though not emphasized so far, the results of the DFT-B3LYP calculations have been shown in parallel to the results of more accurate, though more expensive, MCQDPT calculations (see Sec. III) which we performed on the DFT-optimized structures. As is evident from Figs. 4, 7, and 9, the two sets of data agree well with each other, the discrepancies being at the most few tenths of eV in few cases. No general trend is found in the comparison, except maybe for a general tendency of the correlated wavefunction calculations to give a larger binding energy than DFT for the graphitic sites, see, e.g., the right panel of Fig. 4. This is particularly evident for the *G* site of the coronene molecule: Fig. 9(d) shows that binding to this site is ∼0.2 eV stronger when computed at the MCQDPT than at the DFT level of theory, and that a corresponding trend is found for the barrier. However, given the limited number of active electrons that could be consistently included in the wavefunction calculations, we doubt that this discrepancy is a manifestation of a true physical effect. This is made more evident in Fig. 10, where the adsorption paths for a second H atom onto the *ortho*, *meta*, and *para* position to the first *G* site are displayed for the two different levels of theory. We chose to focus on this system because of the role it played as a cluster model for graphene (graphite) since Jeloaica and Sidis[65] used it to investigate H atom adsorption on the graphitic sites. As is clear from Fig. 10, the above discrepancy doubles when adsorption proceeds in *para*- but vanishes for the *ortho* site, thereby suggesting that the "extension" of the structure may be a source of error in the MCQDPT calculations.

Finally, we performed few additional calculations of the binding energies with a very different implementation of the DFT-GGA theory, namely a Γ-point, periodic plane-wave calculation using a pure GGA functional as described in Sec. III. We find, for coronene, 1.42 and 0.67 eV for adsorption on the *E* and the *G* site, respectively, which compare very well with the values obtained with the hybrid B3LYP functional, namely 1.42 and 0.61 eV. The same holds for the adsorption of a second atom on the same sites considered in Fig. 10: we obtain 2.04, 0.70, and 1.82 eV for the *ortho*, *meta*, and *para* graphitic sites, to be compared with 2.05, 0.69, and 1.65 eV. Notice that also in this case the larger discrepancy occurs at the *para* position, which might signal the need of additional care in the correlation problem.

V. SUMMARY AND CONCLUSIONS

We considered atomic hydrogen adsorption on a number of small graphenic structures (PAH molecules) in order to investigate the enhanced reactivity of the edge sites already observed by several authors. To this end, we selected only small structures to prevent the formation of radical species at the edge, as it occurs with the formation of zero-energy states at the edges of large zigzag nanoribbons. Surprisingly, we found that some edge localization always occurs as a consequence of the reduced coordination (conjugation) of *E* sites which translates into a lower on-site energy in a renormalized lattice. Further localization occurs when *E* sites are highly coordinated in the renormalized lattice, as measured by a "hypercoordination" number ξ. We found a very good correlation between the binding (barrier) energies and the coordination

and hypercoordination numbers: the most favoured sites for H atom adsorption (but likely for adsorption of any monovalent species used to form covalent bonds with carbon) are those showing the lowest coordination and the largest hypercoordination numbers (E' sites in Fig. 2). We also found, similarly to graphene, that further enhancement of the reactivity of specific lattice positions may arise from the same topological frustration which gives rise to midgap states, i.e., that occurring when the maximal set of non-adjacent sites exceeds half of the total number of sites. In this case a preference towards the maximal set of non-adjacent sites adds to the above preference for low coordination and high hypercoordination.

We obtained these results in small (sub-nanometer-sized) graphene structures, but they are expected to hold for more complex structures. For instance, hydrogenation is known to occur much more easily on a zigzag than on an armchair edge of large area graphene, see, e.g., May *et al*.[25] who extrapolated DFT values computed on finite size graphenes towards the infinite size limit and obtained 2.86 $\pm$0.15 eV for the zigzag edge and 1.74 $\pm$ 0.11 eV for the armchair one. This is consistent with the "rules" found here. Indeed, both edges have F and E sites, but only zigzag E sites can be fully hypercoordinated: $\xi = 2$ in this case, to be compared with $\xi = 0$ for the E sites of an armchair edge.

Besides their simplicity, one of the main advantage of the derived rules is that they are based on *local* considerations which hold irrespective of the global electronic properties of the carbon nanostructure under study. As a consequence, our findings suggest that exposing *arbitrarily* shaped graphene dots to controlled amount of atomic hydrogen (e.g., under cold plasma conditions) hydrogenation starts from the edges and propagates into the bulk in a much more efficient way than expected solely on the basis of the bulk adsorption energetics.

[1] K. S. Novoselov, A. K. Geim, S. V. Morozov, D. Jiang, Y. Zhang, S. V. Dubonos, I. V. Gregorieva, and A. A. Firsov, Science **306**, 666 (2004).
[2] A. H. Castro Neto, F. Guinea, N. M. R. Peres, K. S. Novoselov, and A. K. Geim, Rev. Mod. Phys. **81**, 109 (2009).
[3] N. M. R. Peres, Rev. Mod. Phys. **82**, 2673 (2010).
[4] S. Das Sarma, S. Adam, E. H. Hwang, and E. Rossi, Rev. Mod. Phys. **83**, 407 (2011).
[5] K. S. Novoselov, A. K. Geim, S. V. S. V. Morozov, D. Jiang, M. I. Katsnelson, I. V. Gregorieva, S. V. Dubonos, and A. A. Firsov, Nature (London) **438**, 197 (2005).
[6] Y. Zhang, Y.-W. Tan, H. L. Stormer, and P. Kim, Nature (London) **438**, 201 (2005).
[7] A. K. Geim and K. S. Novoselov, Nature Mater. **6**, 183 (2007).
[8] F. Schedin, A. K. Geim, S. V. Morozov, E. W. Hill, P. Blake, M. I. Katsnelson, and K. S. Novoselov, Nature Mater. **6**, 652 (2007).
[9] T. Enoki, Y. Kobayashi, and K.-I. Fukui, Int. Rev. Phys. Chem. **26**, 609 (2007).
[10] Y.-W. Son, M. L. Cohen, and S. G. Louie, Phys. Rev. Lett. **97**, 216803 (2006).
[11] B. Trauzettel, D. V. Bulaev, D. Loss, and G. Burkard, Nat. Phys. **3**, 192 (2007).
[12] M. Ezawa, Phys. Rev. B **77**, 155411 (2008).
[13] W. Sheng, Z. Y. Ning, Z. Q. Yang, and H. Guo, Nanotechnology **21**, 385201 (2010).
[14] W. L. Wang, O. V. Yazyev, S. Meng, and E. Kaxiras, Phys. Rev. Lett. **102**, 157201 (2009).
[15] S. Zhu, J. Zhang, C. Qiao, S. Tang, Y. Li, W. Yuan, B. Li, L. Tian, F. Liu, R. Hu, H. Gao, H. Wei, H. Zhang, H. Sun, and B. Yang, Chem. Commun. **47**, 6858 (2011).
[16] X. Yan, X. Cui, B. Li, and L.-s. Li, Nano Lett. **10**, 1869 (2010).
[17] L. A. Ponomarenko, F. Schedin, M. I. Katsnelson, R. Yang, E. W. Hill, K. S. Novoselov, and A. K. Geim, Science **320**, 356 (2008).
[18] J. Cai, P. Ruffieux, R. Jaafar, M. Bieri, T. Braun, S. Blankenburg, M. Muoth, A. P. Seitsonen, M. Saleh, X. Feng, K. Mullen, and R. Fasel, Nature (London) **466**, 470 (2010).
[19] R. J. Gould and E. E. Salpeter, Astrophy. J. **138**, 393 (1963).
[20] D. Hollenbach and E. E. Salpeter, Astrophy. J. **163**, 155 (1971).
[21] J. Charles W. Bauschlicher, Astrophys. J. Lett. **509**, L125 (1998).
[22] E. Habart, F. Boulanger, L. Verstraete, C. M. Walmsley, and G. Pineau des Forêts, Astron. Astrophys. **414**, 531 (2004).
[23] E. Rauls and L. Hornekær, Astrophys. J. **679**, 531 (2008).
[24] J. A. Sebree, V. V. Kislov, A. M. Mebel, and T. S. Zwier, J. Phys. Chem. A **115**, 6255 (2010).
[25] K. May, B. V. Unterreiner, S. Dapprich, and R. Ahlrichs, Phys. Chem. Chem. Phys. **2**, 5089 (2000).
[26] J. A. Rasmussen, G. Henkelman, and B. Hammer, J. Chem. Phys. **134**, 164703 (2011).
[27] S. Casolo, O. M. Løvvik, R. Martinazzo, and G. F. Tantardini, J. Chem. Phys. **130**, 054704 (2009).
[28] R. Martinazzo, S. Casolo, and G. F. Tantardini, *Physics and Applications of Graphene–Theory* (InTech, Rijeka, Croatia, 2011), Chap. III.
[29] L. Hornekær, E. Rauls, W. Xu, Ž. Šljivančanin, R. Otero, I. Stensgaard, E. Lægsgaard, B. Hammer, and F. Besenbacher, Phys. Rev. Lett. **97**, 186102 (2006).
[30] N. Rogeau, D. Teillet-Billy, and V. Sidis, Chem. Phys. Lett. **431**, 135 (2006).
[31] E. H. Lieb, Phys. Rev. Lett. **62**, 1201 (1989).
[32] J. Fernandez-Rossier and J. J. Palacios, Phys. Rev. Lett. **99**, 177204 (2007).
[33] C. A. Coulson and G. S. Rushbrooke, Mat. Proc. Cambridge Philos. Soc. **36**, 193 (1940).
[34] C. A. Coulson and H. C. Longuet-Higgins, Proc. Roy. Soc. (London), Ser. A **192**, 16 (1947).
[35] R. Martinazzo, S. Casolo, and G. F. Tantardini, Phys. Rev. B **81**, 245420 (2010).
[36] S. Casolo, R. Martinazzo, and G. F. Tantardini, J. Phys. Chem. C **115**, 3250 (2011).
[37] K. Fukui, T. Yonezawa, and H. Shingu, J. Chem. Phys. **20**, 722 (1952).
[38] G. G. Naumis, Phys. Rev. B **76**, 153403 (2007).
[39] The same holds for eigenvectors, see Ref. 35 for details.
[40] M. Inui, S. A. Trugman, and E. Abrahams, Phys. Rev. B **49**, 3190 (1994).
[41] H. C. Longuet-Higgins, J. Chem. Phys. **18**, 265 (1950).
[42] S. Fajtlowicz, P. E. John, and H. Sachs, Croat. Chem. Acta **78**, 195 (2005).
[43] O. V. Yazyev, Rep. Prog. Phys. **73**, 056501 (2010).
[44] M. J. Frisch, G. W. Trucks, H. B. Schlegel *et al*., GAUSSIAN 03, Revision C.02, Gaussian, Inc., Wallingford, CT, 2004.
[45] K. Hirao, Chem. Phys. Lett. **190**, 374 (1992).
[46] K. Hirao, Chem. Phys. Lett. **196**, 397 (1992).
[47] K. Hirao, Int. J. Quantum Chem. **S26**, 517 (1992).
[48] K. Hirao, Chem. Phys. Lett. **201**, 59 (1992).
[49] H. Nakano, K. Nakayama, K. Hirao, and M. Dupuis, J. Chem. Phys. **106**, 4912 (1997).
[50] T. Hashimoto, H. Nakano, and K. Hirao, J. Mol. Struct.: THEOCHEM **451**, 25 (1998).
[51] M. Schmidt, K. Baldridge, J. Boatz, S. Elbert, M. Gordon, J. Jensen, S. Koseki, N. Matsunaga, K. Nguyen, S. Su, T. Windus, M. Dupuis, and J. Montgomery, J. Comput. Chem. **14**, 1347 (1993).
[52] J. Pipek and P. Z. Mezey, J. Chem. Phys. **90**, 4916 (1989).
[53] G. Kresse and J. Hafner, Phys. Rev. B **49**, 14251 (1994).
[54] G. Kresse and J. Hafner, Phys. Rev. B **47**, 558 (1993).
[55] S. Casolo, E. Flage-Larsen, O. M. Løvvik, G. R. Darling, and G. F. Tantardini, Phys. Rev. B **81**, 205412 (2010).
[56] P. E. Blöchl, Phys. Rev. B **50**, 17953 (1994).
[57] G. Kresse and D. Joubert, Phys. Rev. B **59**, 1758 (1999).
[58] J. P. Perdew, K. Burke, and M. Ernzerhof, Phys. Rev. Lett. **77**, 3865 (1996).
[59] For DFT calculations, we refer here to the spin of the Kohn-Sham non-interacting determinant. Spin contamination is always found minimal, i.e., determinants are close to be eigenstates of the total (squared) spin operator, apart from having a well-defined projection.

[60]Y. Ferro, F. Marinelli, and A. Allouche, J. Chem. Phys. **116**, 8124 (2002).
[61]A. Allouche, Y. Ferro, T. Angot, C. Thomas, and J.-M. Layet, J. Chem. Phys. **123**, 124701 (2005).
[62]X. Sha and B. Jackson, Surf. Sci. **496**, 318 (2002).
[63]This is likely due to the importance of next-to-nearest neighboring hoppings which are implicitly included in the *ab initio* calculations and are enough to invalidate Lieb's theorem. These effects might show up in this case because of the presence of supernumerary states, as found in the tight-binding Hamiltonian of the molecule when the added H atom is modeled by a vacancy.
[64]L. Hornekær, Ž. Šljivančanin, W. Xu, R. Otero, E. Rauls, I. Stensgaard, E. Lægsgaard, B. Hammer, and F. Besenbacher, Phys. Rev. Lett. **96**, 156104 (2006).
[65]L. Jeloaica and V. Sidis, Chem. Phys. Lett. **300**, 157 (1999).